Understanding of photocurrent enhancement in real thin film solar cells: towards optimal one-dimensional gratings

Ali Naqavi,[1,2,*] Karin Söderström,[1] Franz-Josef Haug,[1] Vincent Paeder,[2] Toralf Scharf,[2] Hans Peter Herzig,[2] and Christophe Ballif[1]

[1]*Photovoltaics and Thin Film Electronics Laboratory, Institute of Microengineering (IMT), Ecole Polytechnique Fédérale de Lausanne (EPFL), Rue A.-L. Breguet 2, 2000 Neuchâtel, Switzerland*
[2]*Optics and Photonics Technology Laboratory, Ecole Polytechnique Fédérale de Lausanne (EPFL), Rue A.-L. Breguet 2, 2000 Neuchâtel, Switzerland*
**ali.naqavi@epfl.ch*

Abstract: Despite the progress in the engineering of structures to enhance photocurrent in thin film solar cells, there are few comprehensive studies which provide general and intuitive insight into the problem of light trapping. Also, lack of theoretical propositions which are consistent with fabrication is an issue to be improved. We investigate a real thin film solar cell with almost conformal layers grown on a 1D grating metallic back-reflector both experimentally and theoretically. Photocurrent increase is observed as an outcome of guided mode excitation in both theory and experiment by obtaining the external quantum efficiency of the cell for different angles of incidence and in both polarization directions. Finally, the effect of geometrical parameters on the short circuit current density of the device is investigated by considering different substrate shapes that are compatible with solar cell fabrication. Based on our simulations, among the investigated shapes, triangular gratings with a very sharp slope in one side, so called sawtooth gratings, are the most promising 1D gratings for optimal light trapping.

OCIS codes: (040.5350) Photovoltaic; (050.1950) Diffraction gratings; (050.1755) Computational electromagnetic methods.

References and links

1. C. Eisele, C. Nebel, and M. Stutzmann, "Periodic light coupler gratings in amorphous thin film solar cells," J. Appl. Phys. **89**(12), 7722 (2001).
2. N. Senoussaoui, M. Krause, J. Müller, E. Bunte, T. Brammer, and H. Stiebig, "Thin-film solar cells with periodic grating coupler," Thin Solid Films **451**, 397–401 (2004).
3. K. Söderström, F. Haug, J. Escarré, O. Cubero, and C. Ballif, "Photocurrent increase in nip thin film silicon solar cells by guided mode excitation via grating coupler," Appl. Phys. Lett. **96**(21), 213508 (2010).
4. O. Isabella, F. Moll, J. Krč, and M. Zeman, "Modulated surface textures using zinc oxide films for solar cells applications," Phys. Stat. Sol. A **207**, 642–646 (2010).
5. H. Iida, N. Shiba, T. Mishuku, H. Karasawa, A. Ito, M. Yamanaka, and Y. Hayashi, "Efficiency of the a-Si: H solar cell and grain size of SnO transparent conductive film," IEEE Electron Device Lett. **4**(5), 157–159 (1983).
6. T. Söderström, F. Haug, X. Niquille, and C. Ballif, "TCOs for nip thin film silicon solar cells," Prog. Photovolt. Res. Appl. **17**(3), 165–176 (2009).
7. C. Rockstuhl, S. Fahr, K. Bittkau, T. Beckers, R. Carius, F. Haug, T. Söderström, C. Ballif, and F. Lederer, "Comparison and optimization of randomly textured surfaces in thin-film solar cells," Opt. Express **18**(S3), A335–A341 (2010).
8. E. Yablonovitch, and G. D. Cody, "Intensity enhancement in textured optical sheets for solar cells," IEEE Trans. Electron. Dev. **29**(2), 300–305 (1982).
9. P. Sheng, A. Bloch, and R. Stepleman, "Wavelength selective absorption enhancement in thin film solar cells," Appl. Phys. Lett. **43**(6), 579–581 (1983).
10. Z. Yu, A. Raman, and S. Fan, "Fundamental Limit of Nanophotonic Light-Trapping in Solar Cells," in Solar Energy Cells, OSA Technical Digest (CD) (Optical Society of America, 2010), paper PDSWB1.
11. A. Taflove, and S. Hagness, *Computational Electrodynamics: The Finite-Difference Time-Domain Method* (Artech House, 2005) (2010).

#137962 - $15.00 USD Received 9 Nov 2010; revised 10 Dec 2010; accepted 10 Dec 2010; published 21 Dec 2010

12. G. Bao, Z. Chen, and H. Wu, "Adaptive finite-element method for diffraction gratings," J. Opt. Soc. Am. A **22**(6), 1106–1114 (2005).
13. M. Nevière, and E. Popov, *Light propagation in periodic media: differential theory and design* (Marcel Dekker, Inc., 2003).
14. J. Chandezon, M. Dupuis, G. Cornet, and D. Maystre, "Multicoated gratings: a differential formalism applicable in the entire optical region," J. Opt. Soc. Am. **72**(7), 839–846 (1982).
15. L. Li, "Formulation and comparison of two recursive matrix algorithms for modeling layered diffraction gratings," J. Opt. Soc. Am. A **13**(5), 1024 (1996).
16. L. Li, "Use of Fourier series in the analysis of discontinuous periodic structures," J. Opt. Soc. Am. A **13**(9), 1870–1876 (1996).
17. M. Moharam, and T. Gaylord, "Diffraction analysis of dielectric surface-relief gratings," J. Opt. Soc. Am. **72**(10), 1385–1392 (1982).
18. C. Carniglia, "Scalar scattering theory for multilayer optical coatings," Opt. Eng. **18**, 104–115 (1979).
19. A. Poruba, A. Fejfar, Z. Remeš, J. Špringer, M. Vaněček, J. Kočka, J. Meier, P. Torres, and A. Shah, " "Optical absorption and light scattering in microcrystalline silicon thin films and solar cells," J. Appl. Phys. **88**(1), 148 (2000).
20. D. Derkacs, S. Lim, P. Matheu, W. Mar, and E. Yu, "Improved performance of amorphous silicon solar cells via scattering from surface plasmon polaritons in nearby metallic nanoparticles," Appl. Phys. Lett. **89**(9), 093103 (2006).
21. R. Dewan, and D. Knipp, "Light trapping in thin-film silicon solar cells with integrated diffraction grating," J. Appl. Phys. **106**(7), 074901 (2009).
22. N. Feng, J. Michel, L. Zeng, J. Liu, C. Hong, L. Kimerling, and X. Duan, "Design of highly efficient light-trapping structures for thin-film crystalline silicon solar cells," IEEE Trans. Electron. Dev. **54**(8), 1926–1933 (2007).
23. F. Llopis, and I. Tobias, "The role of rear surface in thin silicon solar cells," Sol. Energy Mater. Sol. Cells **87**(1-4), 481–492 (2005).
24. Y. Park, E. Drouard, O. El Daif, X. Letartre, P. Viktorovitch, A. Fave, A. Kaminski, M. Lemiti, and C. Seassal, "Absorption enhancement using photonic crystals for silicon thin film solar cells," Opt. Express **17**(16), 14312–14321 (2009).
25. C. Heine, and R. Morf, "Submicrometer gratings for solar energy applications," Appl. Opt. **34**(14), 2476–2482 (1995).
26. K. Söderström, J. Escarré, F. J. Haug, S. Perregaux, and C. Ballif, "UV-Nano-Imprint Lithography technique for the replication of back reflectors for n-i-p thin film silicon solar cells," Prog. Photo. Res. Appl. (2010).
27. T. Söderström, F. Haug, V. Terrazzoni-Daudrix, and C. Ballif, "Optimization of amorphous silicon thin film solar cells for flexible photovoltaics," J. Appl. Phys. **103**(11), 114509 (2008).
28. N. Chateau, and J. Hugonin, "Algorithm for the rigorous coupled-wave analysis of grating diffraction," J. Opt. Soc. Am. A **11**(4), 1321–1331 (1994).
29. R. H. Morf, "Exponentially convergent and numerically efficient solution of Maxwell's equations for lamellar gratings," J. Opt. Soc. Am. A **12**(5), 1043–1043 (1995).
30. V. Ferry, M. Verschuuren, H. Li, E. Verhagen, R. Walters, R. Schropp, H. Atwater, and A. Polman, "Light trapping in ultrathin plasmonic solar cells," Opt. Express **18**(S2), A237–A245 (2010).
31. P. Johnson, and R. Christy, "Optical constants of the noble metals," Phys. Rev. B **6**(12), 4370–4379 (1972).
32. A. Naqavi, V. Paeder, T. Scharf, K. Söderström, F. Haug, C. Ballif, and H. Herzig, "An RCWA Analysis of Solar Cell Back Reflectors: Comparison between Modelling and Experiment," in *Optical Nanostructures for Photovoltaics, OSA Technical Digest (CD)* (Optical Society of America, 2010)
33. J. Springer, B. Rech, W. Reetz, J. Müller, and M. Vanecek, "Light trapping and optical losses in microcrystalline silicon pin solar cells deposited on surface-textured glass/ZnO substrates," Sol. Energy Mater. Sol. Cells **85**, 1–11 (2005).
34. H. Stiebig, N. Senoussaoui, C. Zahren, C. Haase, and J. Müller, "Silicon thin-film solar cells with rectangular-shaped grating couplers," Prog. Photovolt. Res. Appl. **14**(1), 13–24 (2006).
35. C. Haase, and H. Stiebig, "Thin-film silicon solar cells with efficient periodic light trapping texture," Appl. Phys. Lett. **91**(6), 061116 (2007).
36. S. Zanotto, M. Liscidini, and L. Andreani, "Efficiency Enhancement in Thin-Film Silicon Solar Cells with a Photonic Pattern," in *Optical Nanostructures for Photovoltaics, OSA Technical Digest (CD)*, (Optical Society of America, 2010)
37. S. Zanotto, M. Liscidini, and L. Andreani, "Absorption Enhancement and Light Trapping Regimes in Thin-Film Silicon Solar Cells with a Photonic Pattern," in *2010 Conference on Lasers and Electro-Optics (CLEO) and Quantum Electronics and Laser Science Conference (QELS)*, (Optical Society of America, 2010)

1. Introduction

Solar cells are and attractive route towards sustainable production of electricity; among the various technologies, thin film silicon is particularly attractive because of low material usage and the availability of advanced manufacturing technology. However, the poor electric transport properties necessitate cell thicknesses below the optical absorption length in the red and the infrared part of the spectrum both in amorphous and microcrystalline cells. The main

#137962 - $15.00 USD Received 9 Nov 2010; revised 10 Dec 2010; accepted 10 Dec 2010; published 21 Dec 2010

problem with thin film silicon solar cells is therefore the coupling and confinement of incident light into very thin absorber layers.

Much effort has been devoted to the trapping of light in the cell through periodic [1–4] and random interface textures [5–7], resulting in an effective prolongation of the absorption length. Assuming Lambertian scattering at the interfaces of a low absorbing thin film semiconductor, Yablonovitch suggested an upper limit of the light path enhancement equal to $4n^2$, where n is the refractive index of the absorber film [8]; in the experiment, this limit has not yet been reached. Actually, it has been proposed that periodic structures can even surpass the mentioned limit in a narrow wavelength range [9,10]. However, in solar cells, the absorption enhancement is required to work in a relatively broad spectral range.

An exact knowledge of the steady-state electromagnetic field inside a stack of thin layers with textured interfaces is essential for an assessment of the absorption enhancement. Electromagnetic simulations are thus of great importance in optimizing geometrical parameters such as the shape of the structure and thickness of the layers since they can provide the information about the near field phenomena, most of which are not accessible in the experiment. A fast and stable simulation tool for the prediction of light absorption in multi-layer stacks is hence of great benefit. Full numerical methods such as finite difference time domain (FDTD) [11] and finite element method [12] can be used to obtain the electromagnetic field profile of a specific structure at a pre-defined frequency but they are not appropriate for an optimization due to unacceptable requirements of time or memory. Therefore, semi-analytical methods such as the differential method [13], the coordinate transformation method (C method) [14] and the rigorous coupled wave analysis (RCWA, also called Fourier Modal Method, FMM) [15–17] are preferred. Also, approximate solutions such as scalar scattering theory [18,19] can be used to get an initial insight but they rely on approximations that may not always be fulfilled, and they are normally not capable of handling polarization-dependent effects.

A variety of simulations were performed in regard to solar cells in the past decades, using all the above mentioned theories. Actually, the selection of the simulation method often depends on the problem to be solved. If one is going to investigate the near field phenomena for a specific structure or if the degrees of freedom are reduced, full numerical simulation methods can be used [20,21]; otherwise, one can benefit from the speed of semi-analytical solutions [22–25]. Common to most simulation approaches is the restriction to idealized structures e.g. ideal sinus or binary gratings which is sometimes a significant drawback from an experimental point of view.

In this paper, we present measured photocurrent enhancement of a thin film solar cell with textured interfaces and we compare the results to theoretical predictions using the geometrical parameters that fit well with the experimental measurements. The texture is based on a metallic 1D grating that permits validation of the theory, including the effects that are related to the orientation of the grating lines with respect to polarization. Subsequently, we apply the modeling to explore the ideal structures like sinusoidal, triangular and binary gratings.

2. Experimental

The investigated device is a single junction amorphous silicon solar cell grown on a one-dimensional grating substrate that serves as textured back reflector and is made using the nanoimprint technique described in [26]. A SEM micrograph of the cell is shown in Fig. 1. The substrate grating has a period of 560 nm and the peak to valley depth is 140 nm. It is covered with 120 nm of silver and 60 nm of zinc oxide by sputtering (Univex 450B, Leybold). The solar cell is grown with an n-i-p sequence by very high frequency plasma enhanced chemical vapor deposition, more information are published elsewhere (see for example Ref [27].). When deposited on a flat reference substrate, the nominal thicknesses are 13 nm for the n-layer (n-Si), 200 nm for the i-layer (i-Si), and 17 nm for the p-layer (p-Si). The front contact is made of sputtered indium-tin oxide (ITO), its thickness of 60 nm is designed to yield to an anti-reflection (AR) effect at a wavelength of 550 nm. The absorption enhancement of the grating substrate is investigated by measuring the dependence of the EQE on the incident

#137962 - $15.00 USD Received 9 Nov 2010; revised 10 Dec 2010; accepted 10 Dec 2010; published 21 Dec 2010

angle of the incoming light for P- and S polarizations using a broadband wire polarizer (Proflux PPL05C, Moxtek). Further experimental details can be found in Ref [3]. Note that throughout this paper we use the grating notation where the P polarization refers to the case where the electric field vector is parallel to the grating grooves and S polarization stands for the case where the magnetic field vector is parallel to the grooves.

3. Model

3.1 Electromagnetic field calculation

Among the methods for simulation of grating structures, the RCWA is selected. The main advantages of this method are its speed, simplicity, and generality. In its most fundamental form, RCWA applies Maxwell's equations to the problem of a single 1D binary grating. More complicated structures can be made using a stack of such simple gratings. For the case of 1D binary grating, one can conclude the following relation from Maxwell equations in P polarization [28]

$$\frac{d}{dz}\begin{bmatrix} E_y(z) \\ H_x(z) \end{bmatrix} = [\mathbf{M}]\begin{bmatrix} E_y(z) \\ H_x(z) \end{bmatrix}. \tag{1}$$

In the above relation **M** represents a matrix which depends on the permittivity and E_y and H_x are the Fourier coefficients of the only nonzero component of the electric field and the component of the magnetic field along the direction of periodicity respectively. The directions are shown in Fig. 1. Using eigenvalue decomposition of **M**, the following propagation equation is obtained inside the grating region.

$$\begin{bmatrix} E_y(z_1) \\ H_x(z_1) \end{bmatrix} = [\mathbf{P}]\exp\{(z_1 - z_2)[\mathbf{D}]\}[\mathbf{P}]^{-1}\begin{bmatrix} E_y(z_2) \\ H_x(z_2) \end{bmatrix}. \tag{2}$$

Outside the grating, in the illumination medium and the transmission medium, the field can be expressed via Rayleigh expansion [13]. Therefore, appropriate boundary conditions can be obtained with the continuity of the tangential components of the electromagnetic field.

For extension of the method to a stack of binary gratings, a recursive algorithm has to be used [15,28] or a large but sparse system of equations should be solved [29]. In this paper, we use the recursive approach described in reference [28].

In S polarization, the method can be implemented quite simply by replacing E_y with H_y and H_x with E_x; however, the convergence of the method is poor especially in the case of metallic gratings. One major modification that should be implemented to make convergence faster is applying the Fourier factorization rules [16].

Even after the latter modification, the convergence in S-polarized case is not as good as its P-polarized counterpart. One can mitigate the problem of convergence by coarser staircase approximation at the expense of accuracy.

3.2 Calculation of solar cell parameters

In a solar cell, the quantities that give the most accessible information on absorption enhancement are the total absorption and the external quantum efficiency (EQE). The first one is determined by 1-*R*-*T* where *R* and *T* are total reflection and transmission, respectively. The EQE expresses how many charge carriers are collected with respect to the incident photon flux in short-circuit condition; it is thus a direct measure of the absorption in the intrinsic absorber layer (assuming all carriers are collected); power lost due to parasitic absorption in the metal contact as well as the p-Si and n-Si layers do not contribute to EQE. The EQE can

#137962 - $15.00 USD Received 9 Nov 2010; revised 10 Dec 2010; accepted 10 Dec 2010; published 21 Dec 2010

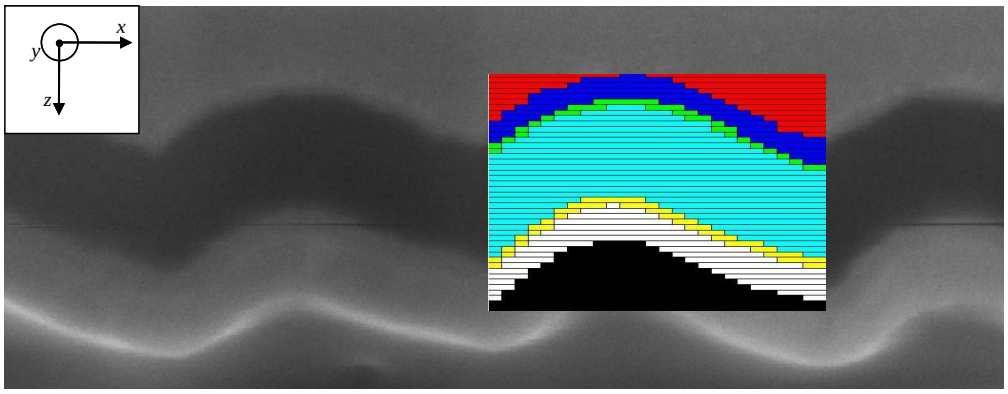

Fig. 1. SEM micrograph of the experimental sample. Thickness of layers is as follows. ZnO = 70nm, ITO = 50nm, i-Si = 180nm, p-Si = 15nm and n-Si = 20 nm. Period of the grating is 550 nm and its peak to valley amplitude is 150nm. The plot shows the approximate structure used in S-polarized simulations. Different colors correspond to different layers; silver, ZnO, n-Si, i-Si, p-Si and ITO are shown in black, white, yellow, cyan, green and blue respectively.

be approximated by calculating the ratio of the energy absorbed in the intrinsic silicon layer to the total incident energy.

$$EQE \simeq \left(1-\eta_r-\eta_t\right).\frac{\iint\limits_{S=i-Si} \varepsilon_i \left|\mathbf{E}\right|^2 dS}{\iint\limits_{S=cell} \varepsilon_i \left|\mathbf{E}\right|^2 dS}. \tag{3}$$

In the latter relation η_r and η_t stand for the diffraction efficiency [13] in reflection and transmission respectively and ε_i represents the imaginary part of the permittivity. Note that this definition represents an upper limit approximation to the EQE; the experimental values are lower because of recombination losses. The short circuit current density, J_{sc}, is determined from the EQE by multiplying it with the illumination spectrum and subsequent integration.

4. Validation of the model, observation of guided modes and their angular variation

Most simulations deal with ideal structures like perfect sinusoidal or binary gratings, and they assume the layers to be perfectly conformal. In practice, there are always deviations from perfect conformal shapes [30]. In this section, we validate the calculation routine using the interface structure of the real device as shown in Fig. 1, i.e. taking into account the flattening of features as they get overgrown with layers of finite thickness. The simulation procedure starts with the characterization of the cell parameters i.e. the thickness of different layers by comparing experimental and theoretical results under P-polarized normal illumination. For the ITO, ZnO, and the silicon layers we use permittivity values that are determined in-house by spectroscopic ellipsometry, whereas literature data are used for the silver layer [31]. To reach acceptable agreement between experiment and theory, we adapt the individual layer thicknesses from the nominal thicknesses of flat reference films that are given in the experimental part; we use 60, 15, 180, 20, and 70 nm for ITO, p-Si, the intrinsic absorber layer (i-Si), n-Si and the ZnO buffer layer, respectively. The silver layer of the back reflector is assumed to be semi-infinite. Furthermore, deviations from full conformality as shown in Fig. 1 are taken into account in the simulation.

Figure 2 shows the experimental and theoretical values of EQE vs. wavelength for both polarizations under normal incidence and Fig. 3 exhibits the same result as Fig. 2 for different angles of incidence. Angular dependence of EQE has been measured/ calculated by changing the incident angle from –50° to + 50° by steps of 10°. Figure 3 illustrates that the theoretical values of the angle resolved EQEs reproduce the dominant variation of the experiment. The

#137962 - $15.00 USD Received 9 Nov 2010; revised 10 Dec 2010; accepted 10 Dec 2010; published 21 Dec 2010

EQE peaks in Fig. 3 and their shift as a function of incident angle can be explained by guided mode excitation [3,32]. The overall better agreement between theory and experiment in P polarization is the result of several phenomena. Firstly, the structure is sliced more coarsely in S polarization to accelerate the simulations. Secondly, despite applying the Fourier factorization rules, light intensity distribution suffers less from Gibbs phenomenon in P polarization. As previously noticed in [3] and confirmed here by modeling, the S-polarized response provides a higher EQE increase in the almost-normal incident angles, but a significant increase on the P-polarized EQE is observed for highly off-normal incidence. The latter observation can be interpreted as the difference in the coupling efficiency of different guided modes [3]. To provide a better feeling of the impact of guided mode excitation approach, we can compare the experimental and the theoretical values of J_{sc} for the sample and its counterpart with flat interfaces. Experimental values of J_{sc} are 11.8 mA/cm^2, 12.95 mA/cm^2 and 10.63 mA/cm^2 for the P- and S polarizations and for the flat substrate respectively [3]. The corresponding theoretical values are 11.65 mA/cm^2, 13.60 mA/cm^2 and 10.97 mA/cm^2 respectively.

The SEM cross section micrograph in Fig. 1 shows that the structure is not symmetric but exhibits a blaze angle. Therefore, both positive and negative angles have been investigated in order to compare the experiment with the theory; the experimental EQE curves are surprisingly symmetric for both polarization directions. In case of the theoretical curves, the P polarization is rather symmetric while certain deviations are observed in the S-polarized case.

To provide a better understanding of the role of different layers in the EQE curve, we briefly discuss the impact of changes in individual layer thicknesses. Generally, the blue response up to the wavelength of 550 nm is dominated by absorption losses in the ITO and in the p-Si layer. Additionally, increasing (decreasing) the ITO thickness shifts the AR condition to longer (shorter) wavelengths, similarly to the case of flat interfaces. The response at long wavelengths is dominated by a Fabry-Perot interference fringe associated with the total silicon thickness close to 600 nm and signatures of several guided modes. The most prominent guided mode is observed for perpendicular incidence and P polarization at 690 nm; in S polarization there are several resonances between 650 and 700nm. The interference fringe as well as the guided modes is most significantly influenced by the thickness of the silicon layers. Because of the high refractive index, thicker layers generally move all features towards longer wavelengths.

Increasing (decreasing) the grating depth generally leaves the positions of guided mode resonances unchanged, but strengthens (weakens) the light absorption associated with a given resonance. Likewise, lengthening (shortening) the grating period shifts the resonance to longer (shorter) wavelengths.

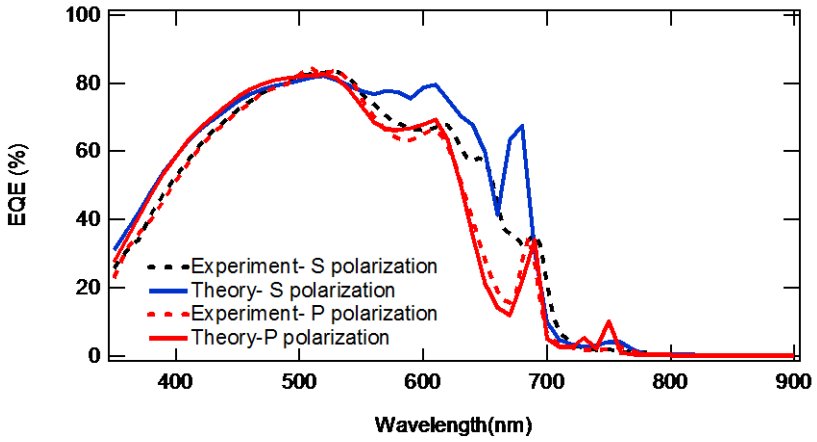

Fig. 2. Comparison of EQE obtained from experiment and theory in both polarizations under normal incidence.

#137962 - $15.00 USD Received 9 Nov 2010; revised 10 Dec 2010; accepted 10 Dec 2010; published 21 Dec 2010

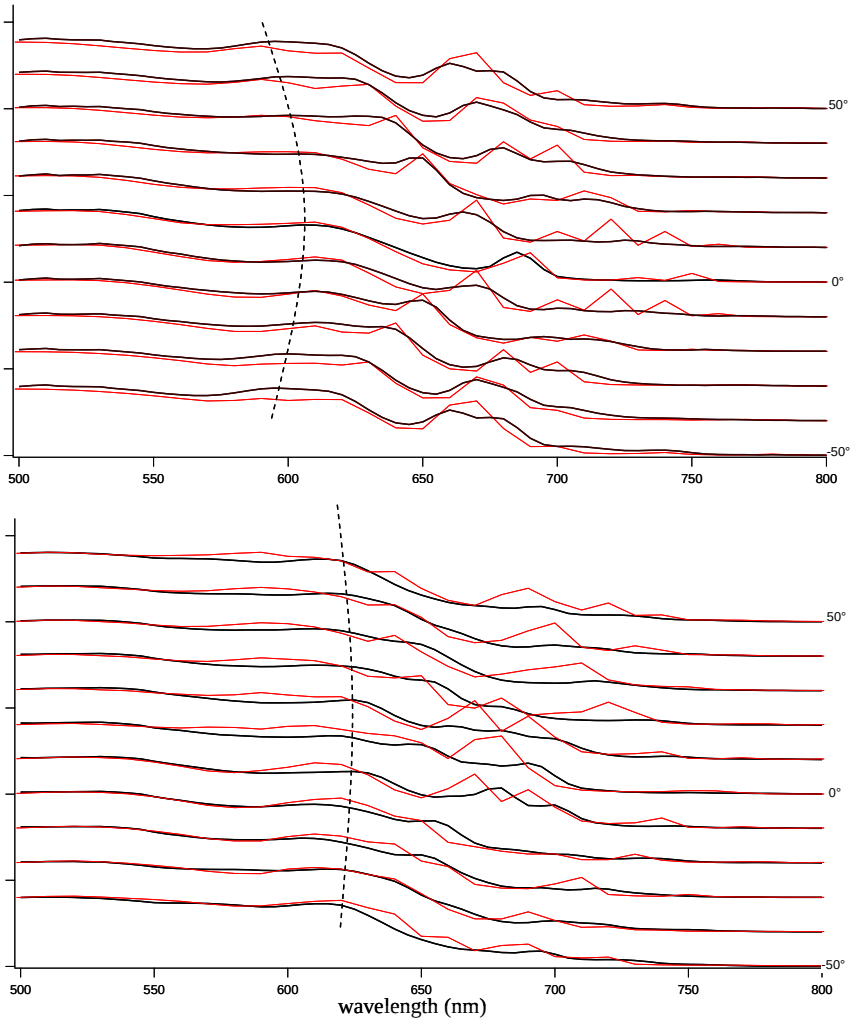

Fig. 3. Angular variations of EQE vs wavelength. The red curves are theoretical results and the black curves are the experimental ones. (up): P polarization, (bottom): S polarization. The dashed line shows the angular variation of interference.

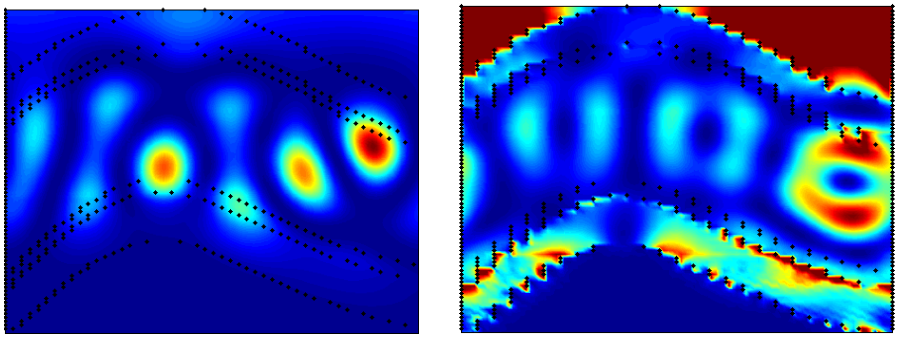

Fig. 4. Normalized intensity profile for the experimental sample in P- (left) and S polarization (right) at 690 nm.

#137962 - $15.00 USD Received 9 Nov 2010; revised 10 Dec 2010; accepted 10 Dec 2010; published 21 Dec 2010

Figure 4 shows the intensity profile at 690 nm for both polarizations. The peak observed in the EQE in P polarization at about 690 nm can be interpreted as a result of presence of a guided mode, i.e. light confinement in the i-Si layer as it is demonstrated by Fig. 4. Also, in S polarization, EQE is relatively high since a large portion of intensity is localized in i-Si layer. As Fig. 4 shows, there is quite some intensity in the silver and at the silicon-ITO interface which leads to EQE drop. Since the field distribution is available all over the structure, one can evaluate the role of different layers in EQE reduction separately. The calculated values of EQE drop associated with the profile of Fig. 4 are 0.02%, 3% and 14% due to absorption in silver, p-Si and ITO respectively. Furthermore, there is a region of high light intensity near the p-Si layer which might not be as useful as it seems in our simulations because the electronic properties of the materials are affected near the interface. This can justify, to some extent, the difference between theory and experiment around 680 nm in Fig. 2 and similar issues in Fig. 3. If field intensity is mainly localized in regions with high charge recombination, i.e. near p-Si or n-Si layer, optical simulation can serve only as an upper limit for the EQE since electronic losses are not included in it.

5. Impact of geometry

After justification of the computational method for both polarizations by comparing the theory with the experimental observations, we apply the model to different back-reflector shapes and discuss the impact on the absorption enhancement. Four different general shapes of 1D gratings are discussed in this manuscript which are plotted in Fig. 5. Short circuit current density serves as a figure of merit for this purpose since it integrates the information about both cell structure -EQE- and solar spectral irradiance; hence, we discuss the impact of geometrical parameters on J_{sc} in different back reflector shapes. Note that to simplify the calculations the simulations are performed under the assumption of normal incidence of light.

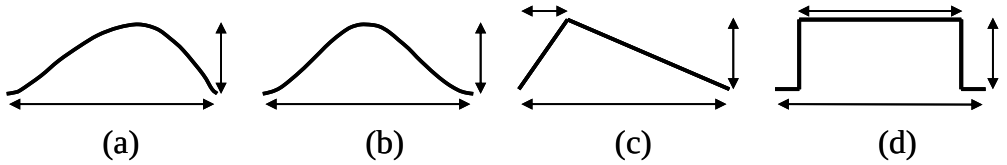

Fig. 5. Four different types of back-reflector grating; a: sawtooth (experimental sample), b: perfect sinusoidal, c: perfect sawtooth and d: binary. Only one period of the back-reflector is shown and the parameters that change are exhibited in each case by arrows.

5.1 Sawtooth and sinusoidal comparison

We consider two geometries; the first one is the sawtooth grating geometry with real interfaces of the previous section (Fig. 5-a), but scaled in depth and period, the second one is a perfect sinusoidal back-reflector with conformal layers (Fig. 5-b). The thicknesses of layers on the sinusoidal grating are assumed to be the same as the respective thicknesses mentioned in the previous section for the experimental sample.

The grating periods are varied from 300 to 800 nm, the peak to valley depths are changed from 50 to 250 nm. The short circuit current densities obtained through the RCWA simulation are depicted in Fig. 6 and Fig. 7 for both polarizations for the sawtooth (experimental sample with scaled dimensions) and sinusoidal shapes, respectively. Overall, the sawtooth grating exhibits higher photocurrents in a wider parameter space than the sinusoidal grating, and it provides a better overlap of high-J_{sc} regions for the two polarizations. Finally, periods between 400 and 600 nm with depths ranging from 175 to 225 nm are altogether acceptable from the point of view of manufacturing and solar cell processing.

It is of interest to move towards ideally sawtooth gratings (Fig. 5-c). As it will be discussed later in more detail in section 5.3 of this contribution, the pure sawtooth grating can result in higher J_{sc} when it has one side as steep as possible. We have simulated such a structure with the sawtooth edge positioned in 10% of the period, assuming the same

#137962 - $15.00 USD Received 9 Nov 2010; revised 10 Dec 2010; accepted 10 Dec 2010; published 21 Dec 2010

thickness of layers as in the previous examples. Figure 8 shows the J_{sc} plot when the period and the depth of the grating are changing. It is observed that in the P polarization case, J_{sc} values are not as high as in the previous cases; however, in the S polarization, J_{sc} takes noticeably larger values. Furthermore, the strong overlap of the J_{sc} between the two polarizations might be used beneficially to obtain higher J_{sc} values.

Short circuit current density depends more on the depth of the grating especially in S polarization if the grating is perfectly sawtooth -Fig. 8. However, in the case of sinusoidal grating, J_{sc} is also very sensitive to changes in the period of the grating back-reflector -Fig. 7. The experimental sample represents a compromise between the two aforementioned cases exhibiting both high current densities and appropriate polarization overlap- Fig. 6. By taking the average of the results obtained for S- and P polarization we can obtain the cell performance under unpolarized light as depicted in Fig. 9. It is observed that a cell based on the sample geometry can potentially produce higher photocurrent over a wide parameter space with the maximal value of about 13.2 mA/cm^2 but a cell with sinusoidal geometry produces at most 13.0 mA/cm^2 of photocurrent.

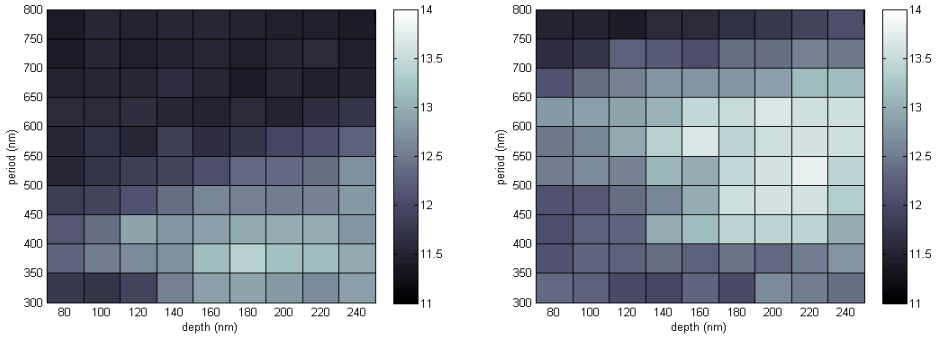

Fig. 6. Short circuit current density variation vs period and depth of grating for P- (left) and S polarization (right). The metallic back-reflector is a sawtooth grating with thicknesses of layers defined in section 4.

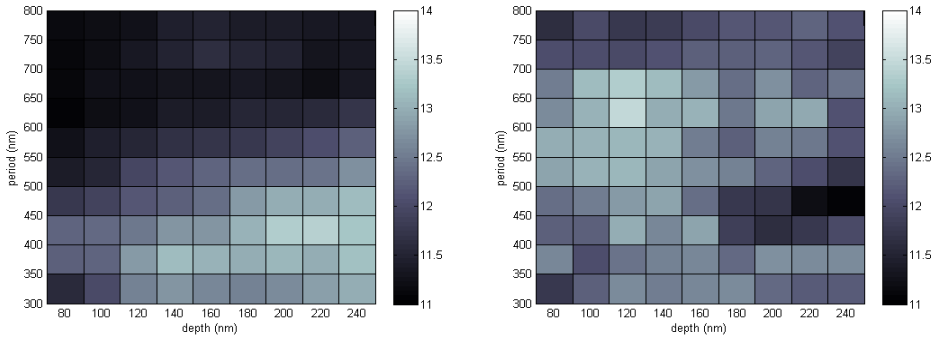

Fig. 7. Short circuit current density variation vs period and depth of grating for P- (left) and S polarization (right). The metallic back-reflector is a sinusoidal grating with thicknesses of layers defined in section 4.

#137962 - $15.00 USD Received 9 Nov 2010; revised 10 Dec 2010; accepted 10 Dec 2010; published 21 Dec 2010

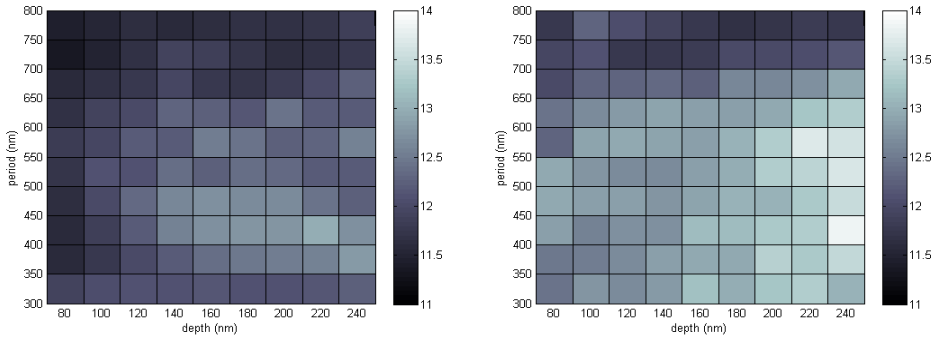

Fig. 8. Short circuit current density variation vs period and depth of grating for P- (left) and S polarization (right). The metallic back-reflector is a perfectly sawtooth grating with thicknesses of layers defined in section 4. Sawtooth edge is positioned at 0.1 of the period.

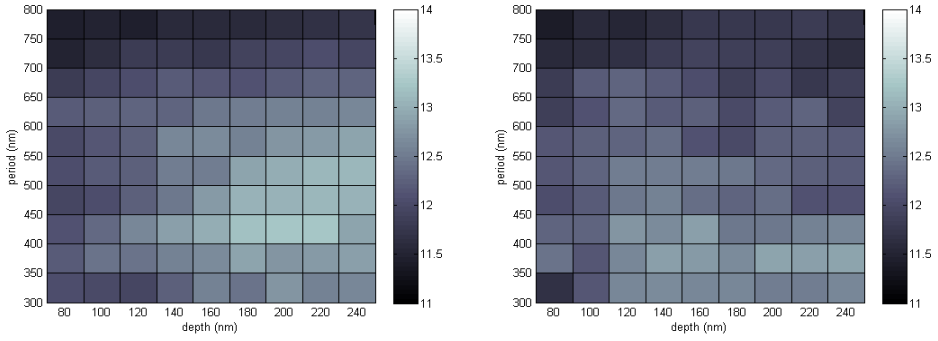

Fig. 9. Short circuit current density variation vs period and depth of grating under unpolarized light for experimental sample (left) and sinusoidal grating (right).

5.2 Blue response behavior

Throughout the geometrical variations of the previous sections, we did not find major improvements in the blue part of the spectrum, despite several reports on an improved coupling of short wavelength light [1,2,33,34]. In this section, we discuss the fact that the potential improvement due to index grading and geometrical AR effect for short wavelengths is overshadowed by the strong absorption in the ITO and in the p-Si.

We distinguish two optical loss mechanisms; there are losses due to reflection (transmission losses are possible but normally taken care of by a back reflector like the silver layer in our configuration). The second loss mechanism is by parasitic absorption in supporting layers that do not contribute to photo-current. Reflection can be greatly reduced by anti-reflection coatings; for example, our cell configuration uses 60 nm of ITO in order to reduce reflection at 550 nm by interference. Interface textures can also be used to reduce reflection because light cannot resolve modulations of the refractive index when their length scale is below the wavelength. For example, Heine and Morf report a broad-band three level zero-order grating that reflects less than 0.37% and 0.52% of the total solar energy flux in P- and S polarization respectively [25]. Also, Haase and Stiebig benefited from pyramidally structured transparent conductive oxide layers to reduce the reflection [35] and they have noticed a compromise between the parasitic absorption loss in the AR coating and its reflectivity in the blue part of the spectrum. Figure 10 compares the AR-properties of our realistic surface structure when its amplitude is varied between 0 (flat interface) and 150 nm (experimental condition). For the flat interface, there is an almost perfect AR condition between ITO and silicon at 500 nm. This interference effect is gradually lost with the

#137962 - $15.00 USD Received 9 Nov 2010; revised 10 Dec 2010; accepted 10 Dec 2010; published 21 Dec 2010

introduction of the surface corrugation; at the same time the reflection is clearly reduced between 350 and 430 nm by the effect of refractive index grading.

Using two representative grating depths of 30 and 150 nm, Fig. 11 illustrates how the AR-effects translate into the EQE; the 30 nm structure exhibits higher values between 480 and 550 nm because the interference effect of the flat interface structure is still applicable to some extent. Below 480 nm, a grating depth of 150 nm results in slightly better EQE due to the effect of refractive index grading. Unfortunately, the AR effect in the blue region turns out to be moderate compared to losses in the ITO and in the p-Si. Figure 11 shows that an upper bound for the EQE is defined by a very simple relation that describes only the absorption in ITO and in the p-Si, without taking into account any reflection effects.

$$EQE_{\max}(\lambda) = \exp\left\{-\frac{4\pi}{\lambda}\left(k_{pSi}d_{pSi} + k_{ITO}d_{ITO}\right)\right\}. \quad (4)$$

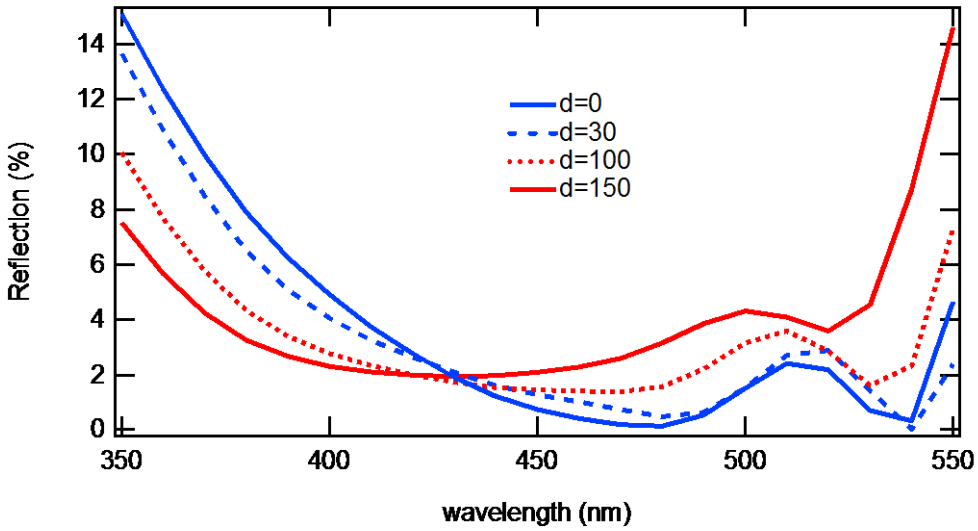

Fig. 10. Reflected power normalized to the incident power (%) for different grating depths. The geometry is similar to the experimental sample but scaled in depth.

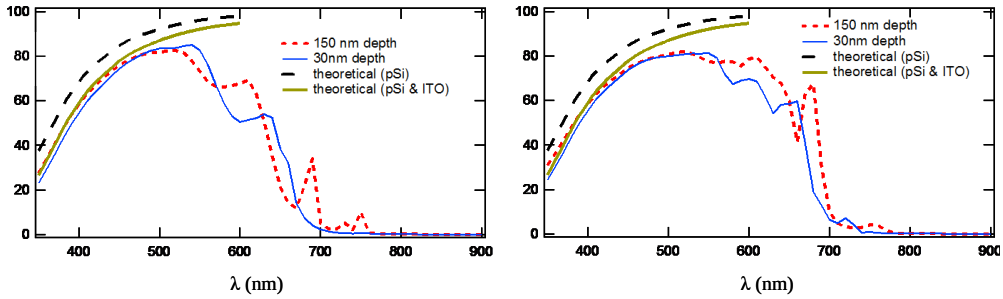

Fig. 11. EQE for two different grating back-reflectors mentioned in section 5.2 for both P (left) and S polarization (right). The absorption in the p-Si alone, and in p-Si and ITO layer is illustrated between 350 and 600 nm by dashed and solid lines respectively.

#137962 - $15.00 USD Received 9 Nov 2010; revised 10 Dec 2010; accepted 10 Dec 2010; published 21 Dec 2010

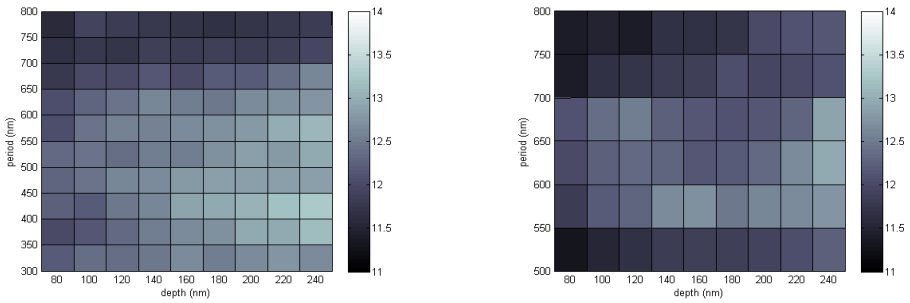

Fig. 12. Short circuit current density variation vs period and depth of grating under unpolarized light for sawtooth grating with sawtooth edge positioned at 0.1 of the period (left) and for binary grating with duty cycle of 0.9 (right).

In Eq. (4), d_{pSi} and d_{ITO} are the thicknesses of p-Si layer and ITO layer which are considered to be 15 and 50 nm, respectively, and k_{pSi} and k_{ITO} are extinction coefficients of the materials at the associated wavelengths.

Figure 11 shows that the absorption losses in ITO are not negligible, but the dominant part of the losses occurs in the p-Si, particularly towards short wavelengths.

5.3 Other geometries

In the next example, two simpler cases are investigated which include ideal structures to provide some insight on the impact of the back-reflector shape. The first case includes an ideal sawtooth grating (Fig. 5-c) and the second one is made on a binary one (Fig. 5-d). The layers of the cell are assumed to be conformal and with the same thicknesses as the experimental sample discussed in the section 4. Degrees of freedom in the first case are period, grating depth and position of sawtooth edge. In the case of the binary shaped back-reflector, the degrees of freedom are the period, the grating depth and the duty cycle of top of the cell. From the simulations, we observe that in the case of sawtooth grating, the high-J_{sc} regions in the two polarizations have a strong overlap. However, the binary shape does not provide this feature. In the latter case, there is no global trend in P polarization to maximize the short circuit current density for specific grating parameters, i.e. there is more than one region of high J_{sc}. Such a splitting of high-J_{sc} regions is not observed in S-polarized case. Clearly defined regions of high current have been reported for unpolarized light on binary patterns [36,37], but the authors used a structure with a flat back-reflector.

The effect of different parameters on the J_{sc} can be described as follows. In the sawtooth grating with shorter period and increased depth and asymmetry brings about higher current. For a binary back-reflector, in P polarization, J_{sc} is more sensitive to change in duty cycle and period than change in grating depth. On the other hand, in S polarization, the impact of depth on J_{sc} is quite obvious as expected; increased depth of grating lets the light couple into the silicon layer more efficiently. Taking the average of P- and S polarization for the two cases of sawtooth and binary gratings, one can obtain the unpolarized J_{sc} as shown in Fig. 12. Note that Fig. 12 shows only a cut of the complete results in the optimal duty cycle/ sawtooth edge position. As observed, the sawtooth grating can show almost the same maximal values of J_{sc} over a wider range of geometrical parameters in comparison with the binary grating. Note that we did not consider periods lower than 500 nm in the case of binary grating; in order to make a meaningful prediction, this would require a detailed analysis of realistic interface structures throughout the device.

We can summarize this section as follows. If the layers are almost conformal as it is the case in real thin amorphous Si solar cells, a sinusoidal shape of metallic back-reflector will result in the poor overlap of optimal regions in P- and S polarizations. A binary shape suffers from the absence of a global optimum and additionally a poor overlap of optimal regions in the two polarizations. The maximum of J_{sc} is higher in S polarization for all of the cases

#137962 - $15.00 USD Received 9 Nov 2010; revised 10 Dec 2010; accepted 10 Dec 2010; published 21 Dec 2010

studied here. A sawtooth shape with as high slope as possible in one side has both a global maximum and very good overlap of the two polarizations. Hence, it seems to be the optimal 1D structure assuming conformal coverage. While sawtooth gratings seem quite good at the first glance, fabrication issues necessarily result in deviations from ideal theoretical designs. In reality, there will probably be some variation from the J_{sc} values predicted by theory due to mismatch between the simulated structures and the fabricated ones and because of the theoretical approximations. Also, realizing grating depths with high aspect ratios, e.g. gratings deeper than 250 nm with a period of less than 400 nm, might be problematic in practice.

6. Conclusion

A real thin film solar cell with almost conformal layers grown on a 1D grating back-reflector is investigated in experiment and theory. Angular variation of EQE is obtained using both experiment and theory to validate the theoretical approach and to show the role of guided modes in enhancing the EQE. To show the impact of different parameters on the short circuit current density, geometrical parameters were changed in the simulations for the experimental sample and for solar cells based on perfect sinusoidal, sawtooth and binary gratings. Grating shape and depth yield different anti-reflective properties for short wavelength, however, in realistic devices, the EQE in that part of the spectrum is found to be dominated by absorption losses and relatively insensitive to anti-reflection effects. RCWA calculations show that among the investigated shapes, sawtooth gratings with a very sharp slope in one side are the optimal 1D gratings for light trapping in near normal incident angles. In practice, however, some deviation from ideal structures is expected.

Acknowledgement

We thankfully acknowledge Dr. Rudolf Morf and David Gablinger from the PSI Villigen for discussions and funding by the Swiss National Science Foundation under project number 200021-125177/1.

#137962 - $15.00 USD Received 9 Nov 2010; revised 10 Dec 2010; accepted 10 Dec 2010; published 21 Dec 2010